Meson production by Δ exchange in $\pi^- p$ interactions at 4 GeV/c

D. L. Scharre,* J. W. Chapman,† R. P. Ely, G. Gidal, W. Michael, and P. Oddone
Lawrence Berkeley Laboratory and Department of Physics, University of California, Berkeley, California 94720
(Received 6 October 1977)

A streamer-chamber spectrometer is triggered by fast forward protons from 4-GeV/c $\pi^- p$ interactions at the Bevatron. Meson-resonance production in the backward, $I_u = 3/2$ exchange reactions $\pi^- p \to p M^-$ are studied, where M^- refers to π^-, ρ^-, A_1^-, A_2^-, and B^-. Elastic scattering and ρ^- production are observed and discussed in detail. No backward A_1^-, A_2^-, or B^- production is observed at the level of approximately 5 μb.

I. INTRODUCTION

This paper reports on an experiment undertaken to analyze backward meson production in 4-GeV/c $\pi^- p$ interactions. A discussion of the backward elastic differential cross section and backward ρ^- production, along with cross-section upper limits for production of A_1^-, A_2^-, and B^- mesons in the backward region, is presented. If standard Regge-exchange phenomenology is applicable, these reactions provide information on pure Δ exchange, as nucleon exchange is forbidden by isospin considerations.

Of particular importance is the question of A_1 meson (the $J^{PC} = 1^{++}$ state required by the standard quark model) production in this experiment. Previous experimental observations of forward produced enhancements in the 1^+ partial wave near 1.1 GeV in mass decaying into $\rho\pi$ have been associated with the A_1 meson.[1] However, the resonance line shape and phase of the 1^+ partial wave relative to slowly varying waves in the same mass region (as determined by partial-wave analysis[2]) is consistent with a Deck-model interpretation.[3] Evidence of A_1 production in a nondiffractive experiment (e.g., charge-exchange, hypercharge-exchange, or baryon-exchange experiment) would support a resonance interpretation of the A_1. No evidence for forward A_1^- production in charge-exchange experiments has been observed.[4] An experiment measuring the recoil missing mass from the proton in the reaction $\pi^- p \to p_{\text{fast}} X^-$ at 8 and 16 GeV/c (Ref. 5) reports enhancements which can be associated with A_1 and A_2 production in the backward region, although the enhancement associated with the A_1 is of low statistical significance. Observation of other mesons in the SU(4) multiplet, of which the A_1 is a member, the Q_A which has been reported in a diffractive $K^* p$ experiment,[6] and the $\chi(3500)$ which is a likely candidate for the $c\bar{c}$ member,[7] make observation of resonant A_1 production imperative.

II. EXPERIMENTAL APPARATUS

A streamer chamber and downstream spectrometer are triggered by fast forward protons resulting from 4-GeV/c $\pi^- p$ interactions. The experimental apparatus is shown in Fig. 1. The beam enters from the left and passes through two planes of beam-defining spark chambers (utilizing magnetostrictive readout) before entering the streamer chamber. The streamer chamber consists of two 20-cm gaps, each 60 × 128 cm. Near the upstream end of the chamber is a 30-cm-long by 2.5-cm-diameter (the approximate diameter of the beam spot) cylindrical liquid hydrogen target. The entire streamer chamber is within a 13-kG magnetic field with the field direction perpendicular to the plane of the diagram in Fig. 1. The trigger system consists of two scintillation-counter hodoscopes on either side of a high-pressure gas Čerenkov counter. The front (back) scintillation counter hodoscope contains 16 (26) counters each 36 in. × 2 in. × 0.375 in. (48 in. × 2 in. × 0.75 in.). The Čerenkov counter has an active area roughly 41 in. in diameter. The momentum of the forward

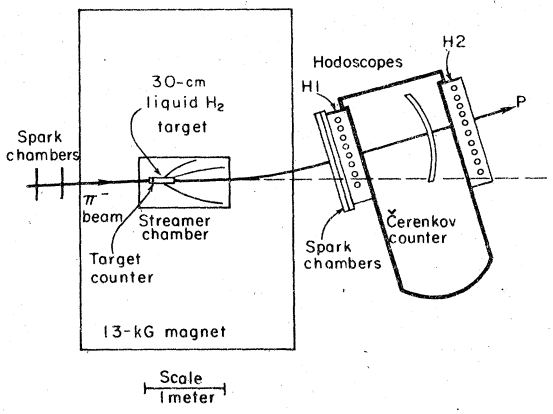

FIG. 1. Experimental apparatus.

particle is crudely determined by the coincidence between counters in the front and back hodoscopes. A hard-wired coincidence matrix requires the momentum of the forward track to be greater than approximately 1.5 GeV/c in order for a trigger to be generated. The Čerenkov-counter signal is required in anticoincidence in the trigger and discriminates against fast-π^+ triggers. The trigger acceptance is adequate for proton recoil mass less than approximately 1.5 GeV over an interval of $\Delta u \simeq 0.4$ GeV^2 (and is greater than 0.80 for recoil mass less than approximately 1.4 GeV over an interval of $\Delta u \simeq 0.2$ GeV^2). Two planes of spark chambers (also utilizing magnetostrictive readout) just upstream of the first hodoscope provide improved resolution on the fast forward track. The active area of these spark-chamber planes is 40.5 in. by 29.0 in. and the wire spacing is 1 mm.

III. CROSS-SECTION CALCULATIONS AND ACCEPTANCES

Approximately 310 000 measurable frames were exposed, representing a sensitivity of nearly 300 events/μb. Eighty percent of the four-prong events and 70% of the two-prong events have been measured and kinematically fitted with versions of TVGP and SQUAW which were modified from standard versions to accomodate the streamer-chamber topology. The changes required involved fitting for the primary vertex position hidden within the target box and correcting the beam and fast forward tracks utilizing the upstream and downstream spark-chamber points. The vertex is defined to be the point within the target which provides the best fit of the extrapolated tracks

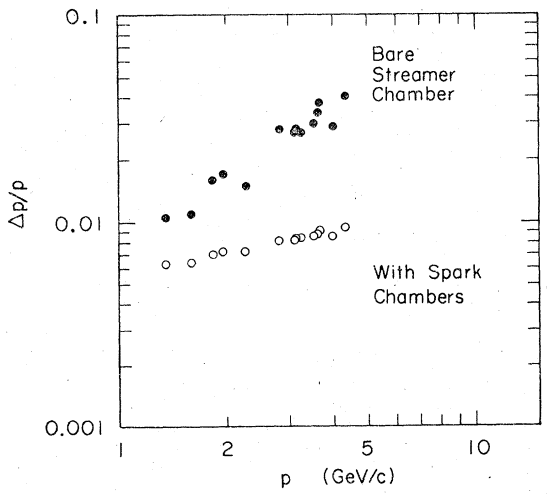

FIG. 2. Fast-forward-track momentum resolution as a function of momentum, with and without downstream spark-chamber points.

to a single point. The external tracks are then extrapolated to this vertex with corrections made to account for energy loss and multiple scattering in the target box. The vertex point and the upstream spark-chamber points are then used to make corrections to the beam track (or create one if it was not measured). The resulting error on the beam momentum is $\Delta p/p \approx 0.7\%$ and the errors on the angles are less than 0.1°. Finally, a fit is made to the fast-forward-track parameters and the downstream spark-chamber points to improve the resolution on the forward track. Figure 2 shows the improvement in momentum resolution for a sample of such tracks. The resulting momentum error is $\Delta p/p < 1\%$ and the angular errors are approximately 0.04° for the azimuth and 0.03° for the dip.

Cross sections are calculated for various reactions using the expression

$$N_{ev}/N_{beam} = \sigma L \rho N_0/A \ ,$$

where

N_{ev} = number of events of interest,
N_{beam} = number of beam tracks passing through hydrogen target,
σ = cross section (cm^2) ,
L = length of the hydrogen target = 27.86 ± 0.14 cm,
ρ = density of liquid hydrogen = 0.0690 ± 0.0005 g/cm^3,
$N_0 = 6.022 \times 10^{23}$ mole^{-1} ,
A = atomic weight of hydrogen = 1.008 g/mole.

The number of beam tracks is corrected for interactions within the hydrogen target box and tracks not traversing the entire length of the target. Corrections for π decay and K^- and $\bar{p}$ contamination in the beam are negligible.

Corrections are applied to the data to account for trigger acceptance and geometric acceptance of the streamer chamber. These corrections are applied to the data on an event-by-event basis. The geometric-acceptance corrections are necessary to correct for event configurations which are unmeasurable or unobservable in a streamer chamber. This includes events in which one or more tracks dips steeply (i.e., has a large relative momentum component along the direction of the applied electric field) so that it becomes very broad and difficult to measure, and events in which one or more outgoing tracks is emitted such that it is obscured from the cameras by the target box. (The problem of flares was minimized by the use of Kodak SO143 high-speed film with special antihalation backing.) Examination of the angular distribution of single tracks shows that tracks outside the region $50° < \theta < 130°$, where θ

is the polar angle from the beam direction, are measurable. Within that region, tracks with ϕ (the azimuthal angle about the beam direction with $\phi = 270°$ toward the cameras) between 60° and 120° or between 240° and 300° are unobservable or subject to poor measurement. All events with a track within this angular region in ϕ are eliminated from the sample of events used in the analysis. To correct for this loss, events with tracks which are in the region $50° < \theta < 130°$, but which are not eliminated, are given a weight inversely proportional to the probability that an arbitrary rotation around the beam axis would yield an event which would be eliminated by the geometric cut. The assumption is made that the physics is independent of the azimuthal angle.

The correction for the trigger acceptance is the most important correction made to the data as the trigger requirement eliminates approximately 95% of the cross section. The experiment was run under two different trigger conditions as determined by the two trigger coincidence matrices. The first 20% of the experiment was run with a fairly loose trigger (with a trigger rate of approximately 2×10^{-3}) and the rest with a tighter trigger (with a trigger rate of approximately 10^{-3}). The first trigger allowed lower-momentum tracks to trigger than the second, and hence, much of the phase space available to a proton from the decay of a forward Δ or N^* was within the acceptance of the system. With the second trigger, a higher proportion of the events accepted corresponded to a relatively low-mass meson system recoiling against the forward proton.

Contours of constant trigger acceptance (uncorrected for topology) as functions of proton laboratory momentum and polar angle (from the beam) for the first and second trigger conditions are shown in Figs. 3(a) and 3(b). The acceptances are calculated by generating tracks originating in the target with a given momentum and polar angle, and swimming the tracks through the magnetic field to the downstream trigger system. A track passing through counters in the front and back hodoscopes yielding a valid coincidence is assumed to have unit acceptance. The generated acceptances are averaged over azimuthal angle and primary vertex position. In order to account for correlations with unobserved tracks (due to flaring or target obscuration), the actual acceptances used in the analysis are topology dependent. The acceptances are calculated by generating entire events corresponding to the topology of interest, and using only the sample of events which are not eliminated by the geometric cut to calculate the acceptance probabilities.

Additional corrections are made to the cross-section normalization for loss of events due to secondary interactions. This includes proton interactions between the hydrogen target and the trigger system and interactions of the other outgoing tracks in the target box. This correction is 8% for two-prong events and 10% for four-prong events. The correction due to scanning and measuring inefficiency losses (22%) was evaluated by rescanning and remeasuring portions of the film. An additional 5% of the events are lost due to software cuts to eliminate contamination.

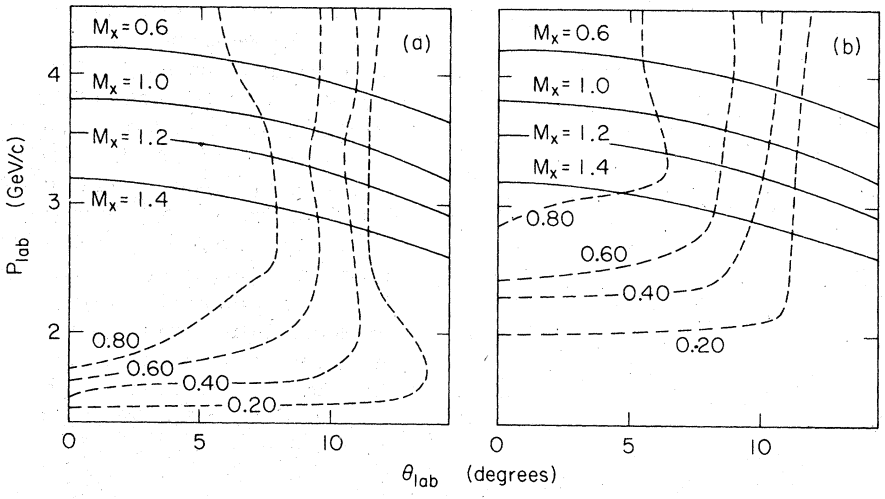

FIG. 3. Trigger-acceptance contours as functions of proton laboratory momentum and polar angle (from the beam direction) for the (a) first and (b) second trigger conditions.

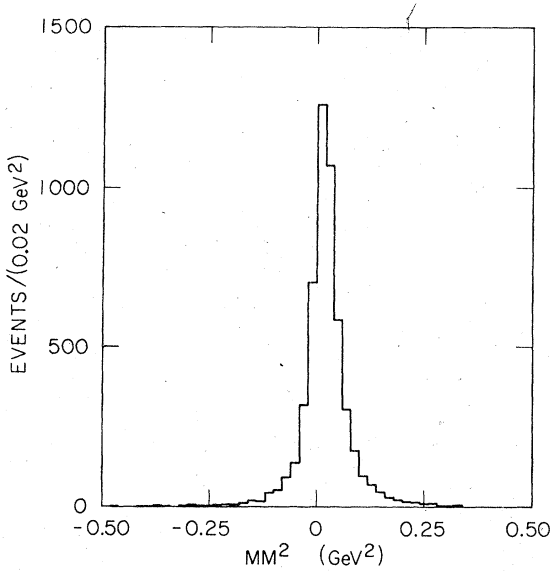

FIG. 4. Missing-mass-squared distribution for events satisfying the reaction $\pi^- p \to \pi^- \pi^- \pi^+ p \pi^0$.

IV. RESULTS

In this paper, analysis of the reaction

$$\pi^- p \to p_{\text{fast}} M^-$$

is discussed, where the meson system M^- is specifically π^-, ρ^-, A_1^-, A_2^-, or B^-. Events satisfying any one of four kinematic hypotheses are used in the analysis. In the sample of two-prong events, there are 458 events which satisfy the four-constraint (4C) hypothesis

$$\pi^- p \to p\pi^- , \tag{1}$$

and 5102 events which satisfy the 1C hypothesis

$$\pi^- p \to \pi^- p\pi^0 . \tag{2}$$

In the sample of four-prong events, there are 4136 events which satisfy the 4C hypothesis

$$\pi^- p \to \pi^- \pi^- \pi^+ p , \tag{3}$$

and 7898 events which satisfy the 1C hypothesis

$$\pi^- p \to \pi^- \pi^- \pi^+ p\pi^0 . \tag{4}$$

Contamination of the event samples due to kinematic ambiguities with competing hypotheses has been found to be minimal (less than a few percent) in the kinematic regions of interest.

The ability to separate different 1C fits is due primarily to the added resolution acquired for the beam track by using two planes of upstream spark chambers and for the forward proton by using the downstream spark-chamber planes. To indicate the level of purity of the event sample, a histogram of the missing mass squared from the charged tracks for the sample of events satisfying (4) is shown in Fig. 4. Contamination of the event sample would manifest itself as a right-left asymmetry of the distribution, which is not observed.[8] In Fig. 5(a) is the kinematic fit χ^2 probability distribution for these same events. Except for the rise at small probability, the distribution is fairly flat. (If a confidence level cut of 0.07 is imposed on the data, the contamination in the event sample is reduced to approximately 1%.) In Fig. 5(b) is the vertex fit χ^2 probability distribution for a sample of four-prong events. The rise at large probability is due to a portion of the events for which the beam position was unknown in the fitting and the errors assigned to the nominal beam position were too large. Otherwise, the distribution appears reasonable.

A. Elastic scattering

The backward elastic differential cross section, as a function of $u' = u - u_{\max}$, is shown in Fig. 6(a)

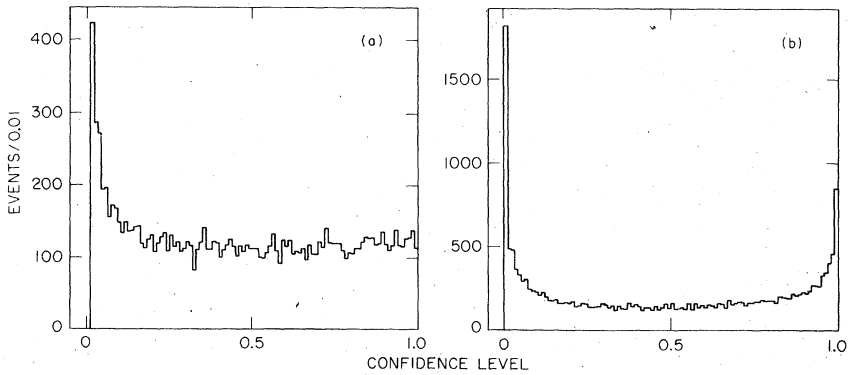

FIG. 5. (a) Kinematic fit and (b) vertex fit χ^2 probability distributions for events satisfying the reaction $\pi^- p \to \pi^- \pi^- \pi^+ p \pi^0$.

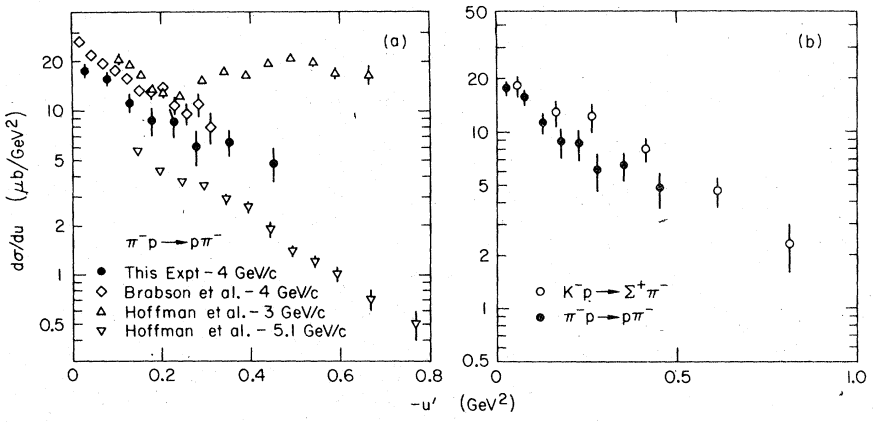

FIG. 6. Differential cross section for $\pi^- p \to \pi^- p$ as a function of u'. (a) Also shown are data of Brabson *et al.* (Ref. 9) and Hoffman *et al.* (Ref. 10). (b) Also shown are data of Massaro *et al.* (Ref. 11).

and in Table I. Also shown in the figure are data from the experiments of Brabson *et al.*[9] at 4 GeV/c and Hoffman *et al.*[10] at 3 and 5.1 GeV/c. All errors shown are statistical only. The data at 4 and 5.1 GeV/c are consistent in structure with the data from this experiment. The data at 3 GeV/c appears to have dip structure and possibly a second maximum, but it is expected that s- and t-channel processes will have more of an effect in the backward region at 3 GeV/c than at higher energies. The overall normalization of the data from this experiment and the experiment of Brabson *et al.* appears to be slightly different, but when systematic errors of both experiments are considered, the results are observed to be consistent. The differential cross section is also compared with the results of a 4.2-GeV/c experiment of Massaro *et al.*[11] [shown in Fig. 6(b)] in which the reaction

$$K^- p \to \pi^- \Sigma^+$$

is examined in the backward direction. This reaction (also requiring Δ exchange) is predicted to be equal to $\pi^- p$ backward elastic scattering by SU(3). Comparison of the two reactions shows this to be approximately true.

TABLE I. $\pi^- p$ backward elastic differential cross section as a function of u'.

$-u'$ (GeV^2)	Δu (GeV^2)	$d\sigma/du$ (μb/GeV^2)
0.025	0.05	17.7 ± 1.7
0.075	0.05	15.7 ± 1.6
0.125	0.05	11.3 ± 1.5
0.175	0.05	8.8 ± 1.7
0.225	0.05	8.6 ± 1.7
0.275	0.05	6.1 ± 1.5
0.350	0.10	6.5 ± 1.2
0.450	0.10	4.8 ± 1.1

A maximum-likelihood fit made to the backward elastic data [reaction (1)] with parametrization

$$\frac{d\sigma}{du} = \sigma_{el} b e^{bu'} \tag{5}$$

results in the following fit parameters (a systematic error of ± 15% is included in the cross section):

$$\sigma_{el} = 5.16 \pm 0.85 \ \mu\text{b} ,$$

$$b = 3.86 \pm 0.40 \ \text{GeV}^{-2} .$$

In Fig. 7(a) are shown the extrapolated total backward elastic cross sections measured in this and previous experiments. Included are data from Hoffman *et al.*[10] at 5.1 GeV/c, Brabson *et al.*[9] at 4 GeV/c, Owen *et al.*[12] at 5.9 GeV/c, and Anderson *et al.*[13] at 8 and 16 GeV/c. The data points include systematic errors and in some cases are calculated in terms of parameters to a fit over a limited range of u.[14] The straight line in Fig. 7(a) is a linear least-squares fit to the data in log-log space. The functional dependence of the total backward cross section with incident laboratory momentum as determined by the fit is

$$\sigma_{el} \propto P_{lab}^{(-2.43 \pm 0.17)} ,$$

where P_{lab} is the laboratory momentum. This is consistent with the s dependence expected by Regge theory for Δ-exchange processes. In Fig. 7(b) are the fitted values of the slope parameter b for this and the other experiments discussed above. The slope is seen to be roughly independent of the incident beam momentum. The consistency of our elastic-scattering results with the results of other

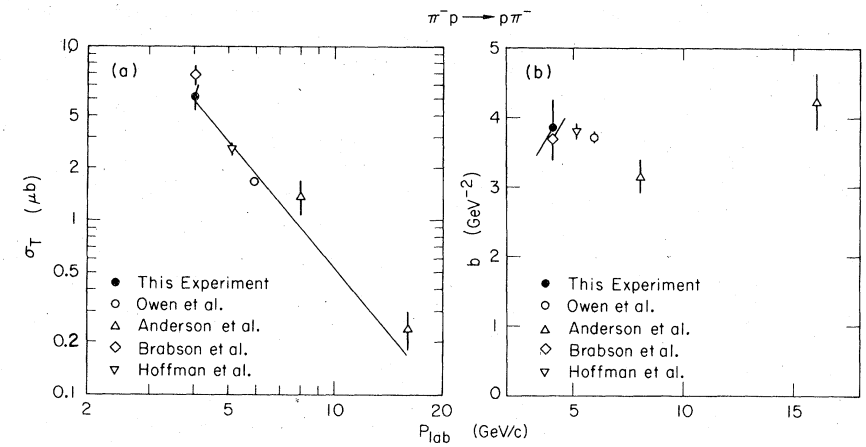

FIG. 7. (a) Total backward elastic cross section and (b) backward slope parameter for $\pi^- p \rightarrow \pi^- p$ as functions of incident beam momentum. Also shown are data of Hoffman *et al.* (Ref. 10), Brabson *et al.* (Ref. 9), Owen *et al.* (Ref. 12), and Anderson *et al.* (Ref. 13). Curve is described in text.

experiments gives us confidence in our normalization and acceptance procedures.

B. ρ^- production

In Fig. 8(a) is the Dalitz plot for the three-body final state [reaction (2)]. The $\pi^-\pi^0$ invariant-mass projection is shown in Fig. 8(b). Significant ρ^- production is observed. The $p\pi^-$ invariant-mass projection is shown in Fig. 8(c). The shaded region represents those events produced in which $\cos\theta^*_{\pi^- \rightarrow p\pi^-} > 0.8$, where $\theta^*_{\pi^- \rightarrow p\pi^-}$ is the center-of-mass production angle between the beam and the

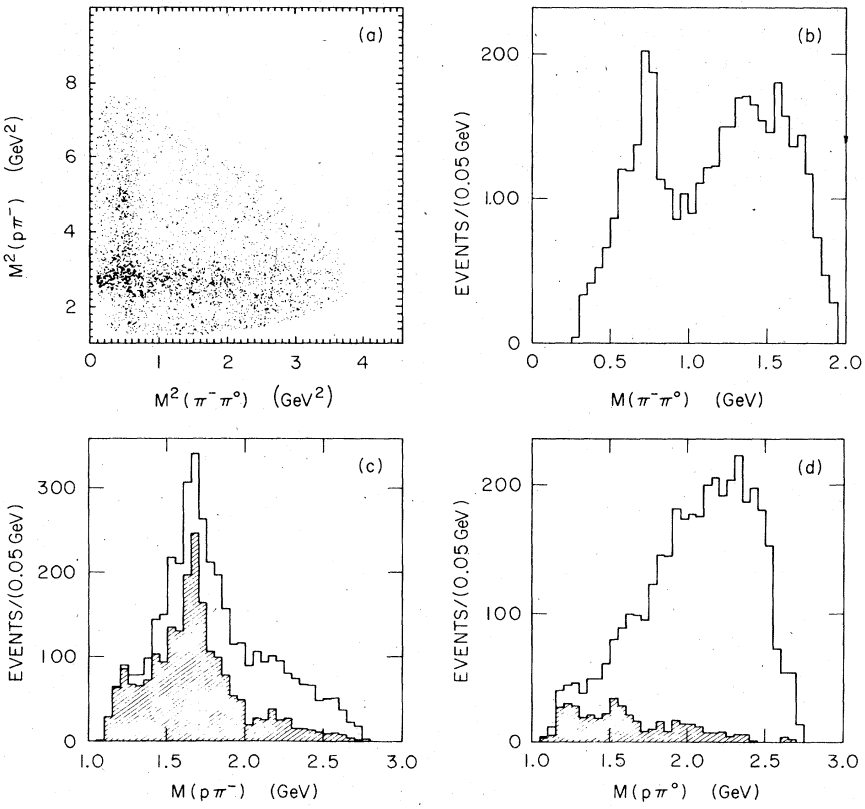

FIG. 8. (a) Dalitz plot for $\pi^- p \rightarrow \pi^- p\pi^0$. (b) $\pi^-\pi^0$ invariant-mass distribution (c) $p\pi^-$ invariant-mass distribution. (d) $p\pi^0$ invariant-mass distribution. See text for details regarding shaded regions.

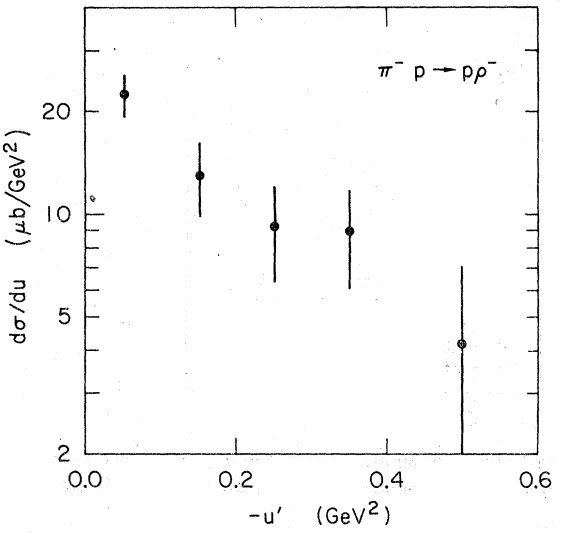

FIG. 9. Differential cross section for $\pi^- p \to p\rho^-$ as a function of u'.

$p\pi^-$ system. Some evidence for $\Delta^0(1232)$ production is observed and evidence for significant production of N^{*0} is observed in the region of 1.6 GeV. In Fig. 8(d) is the $p\pi^0$ invariant-mass projection. The shaded region only includes events in which $\cos\theta^*_{\pi^- \to p\pi^0} > 0.8$. In addition, events in the ρ^- and N^{*0} bands are eliminated. Evidence for $\Delta^+(1232)$ production and possible evidence for higher-mass N^{**} production is observed. A multichannel maximum-likelihood fit to this sample of data has been done (described elsewhere[14]), and shows that reaction (2) is consistent with mostly quasi-two-body production in the final state (i.e., $p\rho^-$ and $N^*\pi$).

TABLE II. Differential cross section for $\pi^- p \to p\rho^-$ as a function of u'.

$-u'$ (GeV^2)	Δu (GeV^2)	$d\sigma/du$ (μb/GeV^2)
0.05	0.10	22.5 ± 3.2
0.15	0.10	13.1 ± 3.2
0.25	0.10	9.3 ± 2.9
0.35	0.10	9.0 ± 2.9
0.50	0.20	4.2 ± 2.9

Analysis of the ρ^- signal is accomplished by fitting the $\pi^-\pi^0$ invariant-mass distribution (corrected for trigger acceptance) to an expression consisting of a Breit-Wigner resonance term above an incoherent background term.[16] The background term is primarily due to N^* production. The resulting fit to the distribution yields a ρ^- with mass $M = 0.737 \pm 0.006$ GeV and with width $\Gamma = 0.088 \pm 0.024$ GeV. The low mass and width of the ρ^- (in conjunction with the results of the maximum-likelihood fit) indicate that interference is taking place between the ρ^- signal and the background. Discussion and detailed analysis of this interference is presented elsewhere.[17]

A background subtraction and correction for the Briet-Wigner tails is made to the data in the ρ^- mass region based on the parameters obtained in the fit. The resulting differential cross section as a function of u' (corrected for loss of events with small trigger acceptance[18]) is given in Fig. 9 and Table II. A least-squares fit to the data points was made using the parametrization of Eq. (5) with the results $\sigma_T = 7.0 \pm 1.6$ μb and $b = 3.7 \pm 1.0$ GeV^{-2}. The errors include the estimated ±15% systematic error, but no correction is made to account for

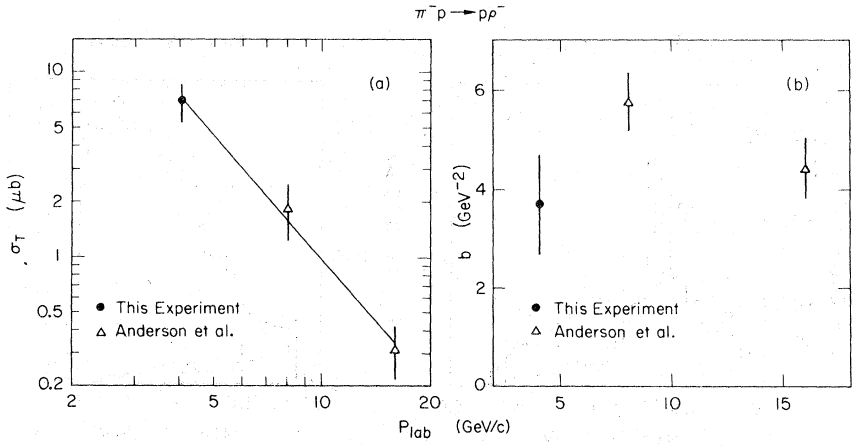

FIG. 10. (a) Total backward cross section and (b) backward slope parameter for $\pi^- p \to p\rho^-$ as functions of incident beam momentum. Also shown are data of Anderson *et al.* (Ref. 19). Curve is described in text.

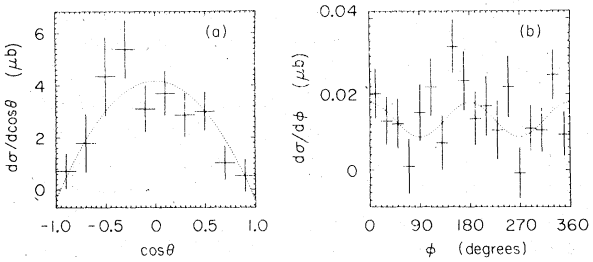

FIG. 11. (a) $\cos\theta$ and (b) ϕ s-channel helicity-frame decay distributions for the ρ^- averaged over $u' > -0.4$ GeV^2.

errors associated with the parameters of the ρ^- resonance (mass and width), the structure of the background, the extrapolation of the parametrization given in Eq. (5) to all values of u', and the assumption of incoherence of the resonant and background cross sections.

In Fig. 10(a) is a plot of the total cross section as a function of incident beam momentum for this experiment and the experiment of Anderson *et al.*[19] and 8 and 16 GeV/c. All data points include systematic errors. The straight line represents a linear least squares fit to the three data points in log-log space. The functional dependence of the total backward cross section with laboratory momentum as determined by the fit is

$$\sigma_T \propto P_{\text{lab}}^{(-2.20\pm0.28)} .$$

The value of the exponent is consistent with the value of 2.43 ± 0.17 obtained in the backward elastic-scattering case. In Fig. 10(b) are fitted values of the slope parameter b for the two experiments as a function of laboratory momentum. No significant deviation as a function of momentum is observed.

TABLE III. ρ^- helicity-frame density matrix elements.

	s channel	u channel
ρ_{00}	-0.05 ± 0.07	0.18 ± 0.09
$\text{Re}\rho_{10}$	-0.03 ± 0.05	0.29 ± 0.06
$\text{Im}\rho_{10}$	-0.05 ± 0.05	0.06 ± 0.06
$\text{Re}\rho_{1,-1}$	-0.17 ± 0.08	-0.06 ± 0.07
$\text{Im}\rho_{1,-1}$	-0.14 ± 0.08	-0.15 ± 0.08

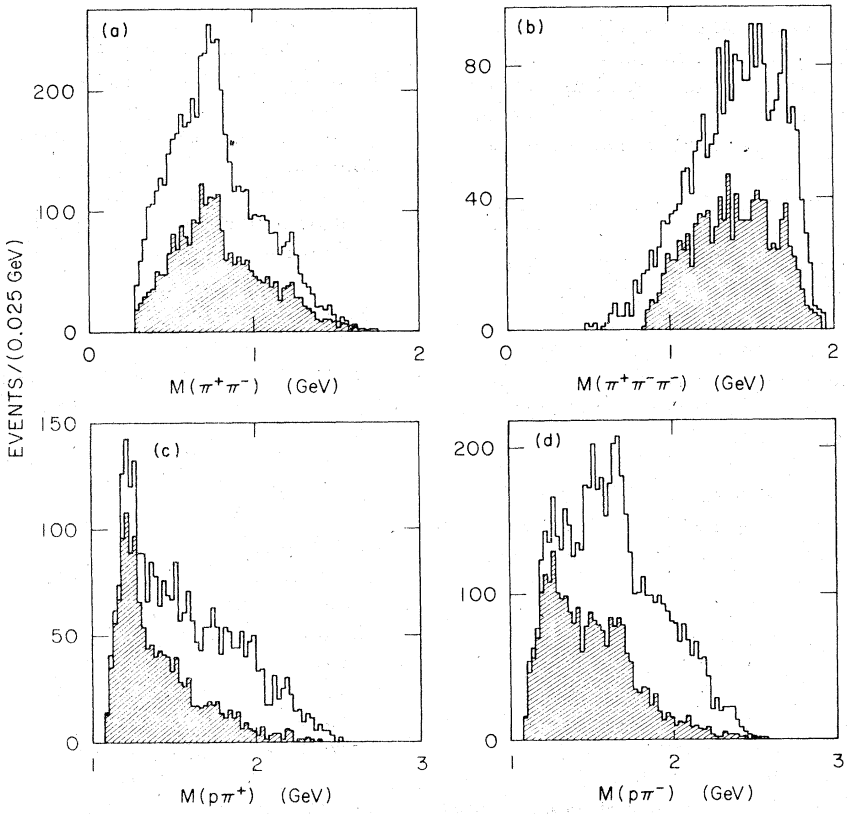

FIG. 12. (a) $\pi^+\pi^-$, (b) $\pi^+\pi^-\pi^-$ (with $\cos\theta^*_{\pi^-\to p} > 0.8$), (c) $p\pi^+$, and (d) $p\pi^-$ invariant-mass distributions for $\pi^- p \to \pi^-\pi^-\pi^+ p$. See text for details regarding shaded regions.

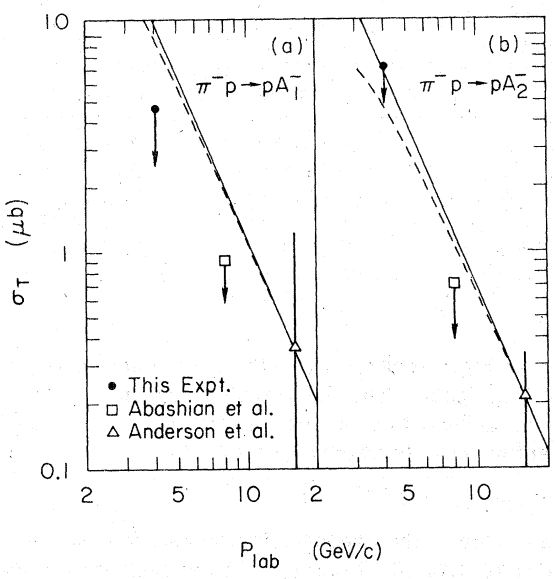

FIG. 13. Total backward cross sections as functions of incident beam momentum for (a) $\pi^- p \to pA_1^-$ and (b) $\pi^- p \to pA_2^-$. Also shown are data of Abashian *et al.* (Ref. 25) and Anderson *et al.* (Ref. 5). Curves are described in text.

As this experiment utilizes a nearly 4π solid angle detector, it is possible to analyze the ρ^- decay angular distribution. In Fig. 11 are shown the distributions for $\cos\theta$ and ϕ in the s-channel helicity frame for events in the ρ^- mass region after background subtraction. The additional requirement is imposed that $u' > -0.4$ GeV^2. Both the Dalitz plot [Fig. 8(a)] and the $\cos\theta$ distributions show that the ρ^- band is crossed by several N^* bands. These N^* decays into $p\pi^-$ can interfere with the ρ decay angular distributions. These interference effects are discussed in another paper,[17] but are mentioned here as a caveat. In this paper, it is assumed that on the average, the background subtracted ρ^- decay distributions are not greatly affected by this interference. In this spirit, we give the ρ^- density matrix elements[20] averaged over the interval $u' > -0.4$ GeV^2 in both the s-channel and u-channel helicity frames in Table III.

C. A^- production

In Fig. 12(a) is the $\pi^+\pi^-$ invariant-mass distribution for the sample of events satisfying reaction (3). The shaded region shows those events in which $\cos\theta^*_{p \to \pi^+\pi^-} > 0.8$. There is a strong ρ^0 signal and evidence for an f^0. In Figs. 12(c) and 12(d) are the $p\pi^+$ and $p\pi^-$ invariant-mass distributions. The shaded regions show those events in which $\cos\theta^*_{\pi^- \to p\pi^\pm} > 0.8$. Evidence for $\Delta(1232)$ and higher-mass N^* production is observed. In Fig. 12(b) is the $\pi^+\pi^-\pi^-$ invariant-mass distribution with $\cos\theta^*_{\pi^- \to \rho} > 0.8$ (this cut corresponds closely to the trigger acceptance cutoff). The shaded region shows those events in which at least one $\pi^+\pi^-$ mass combination is in the ρ^0 mass region (defined to be between 0.675 and 0.825 GeV). There is no evidence for A_1^- or A_2^- production.

In order to obtain cross-section upper limits for A_1^- and A_2^- production, a least-squares fit to the invariant-mass distribution (corrected for trigger acceptance) between 0.8 and 1.5 GeV in mass is made. The distribution is parametrized in terms of a Breit-Wigner resonance term over an incoherent quadratic background. The fitting is done separately for the A_1^- (with an assumed mass of $M = 1.10$ GeV and an assumed width of $\Gamma = 0.100$ GeV) and the A_2^- (with $M = 1.31$ GeV and $\Gamma = 0.102$ GeV). The resulting cross sections are corrected for loss of events with small trigger acceptance,[21] loss of events resulting from the production-angle cut applied to the data,[22] and unobserved decay modes,[23] to yield $\sigma(A_1^-) = 0.5 \pm 2.1$ μb and $\sigma(A_2^-) = 0.8 \pm 3.2$ μb. The resulting 95%-confidence-level upper limits for A_1^- and A_2^- production are $\sigma(A_1^-) < 4.7$ μb and $\sigma(A_2^-) < 7.2$ μb. There is some uncertainty in the A_1^- upper limit resulting from lack of knowledge of the A_1 width and decay modes. Variation of the position of the A_1 mass (for values of mass below approximately 1.35 GeV) does not significantly affect the cross-section upper limit. The measured value of the A_1 cross-section upper limit is larger than the 2-μb theoretical estimate quoted by Haber and Kane.[24] (This can be compared with the theoretical estimate of 7 μb for backward ρ^- production which is consistent with experimental results.)

In Figs. 13(a) and 13(b) are the total backward cross sections for A_1^- and A_2^- production as functions of incident beam momentum. The data points at 4 and 8 GeV/c are the 95%-confidence-level upper limits as determined by this experiment and the experiment of Abashian *et al.*[25] The 16-GeV/c data points are the cross sections (less than a 1.5 standard deviation effect in the case of the A_1^-) as determined by Anderson *et al.*[5] The solid lines are extrapolations from the 16-GeV/c data points to the other values of laboratory momentum with the assumption that the total backward cross section varies as $P_{lab}^{-2.5}$. The dashed curve is an extrapolation in which the "u_{max} effect" is taken into account (i.e., $d\sigma/du$ at $u = 0$ is assumed to vary as $P_{lab}^{-2.5}$). The A_1^- cross-section upper limit is observed to be considerably below the 16-GeV/c extrapolation.

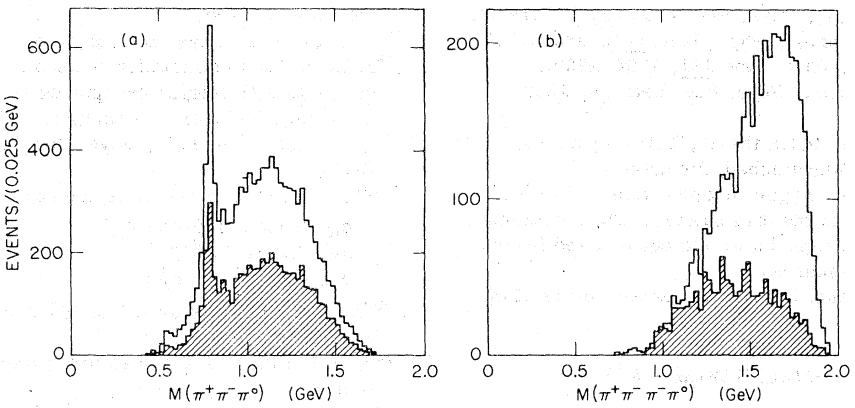

FIG. 14. (a) $\pi^+\pi^-\pi^0$ and (b) $\pi^+\pi^-\pi^-\pi^0$ (with $\cos\theta^*_{\pi^-\to p}>0.8$) mass distributions for $\pi^-p\to\pi^-\pi^-\pi^+p\pi^0$. See text for details regarding shaded regions.

D. B^- production

Most models of the reaction $\pi^+p\to\omega^0\Delta^{++}$ in the forward direction ascribe the unnatural-parity-exchange contribution to a $B\Delta p$ coupling. Although the corresponding theoretical expectation is uncertain, we have searched for backward B production by Δ exchange.

Figure 14(a) shows the $\pi^+\pi^-\pi^0$ invariant-mass distribution for the sample of events satisfying reaction (4). The shaded region includes only those events in which $\cos\theta^*_{p\to\pi^+\pi^-\pi^0}>0.8$. Clear evidence for ω^0 and η^0 production is observed in this final state. This will be discussed in a forthcoming paper in which resonance production in the four- and five-body final states is analyzed (see also Ref. 14). In Fig. 14(b) is the $\pi^+\pi^-\pi^-\pi^0$ invariant-mass distribution with $\cos\theta^*_{\pi^-\to p}>0.8$. The shaded region includes only those events in which at least one $\pi^+\pi^-\pi^0$ mass combination is in the ω^0 mass region (defined to be between 0.735 and 0.835 GeV). No evidence of B^- production is observed. The cross-section upper limit is calculated in the same manner as for the A_1^- and the A_2^-. The resulting 95%-confidence-level cross-section upper limit[26] is $\sigma(B^-)<4.1$ μb. This upper limit includes all corrections for unobserved decay modes and assumes a fall-off with u' as $e^{3tu'}$.

V. CONCLUSIONS

In conclusion, measurements of Δ-exchange production of π^- and ρ^- in the backward region are presented. One also expects A_2^- and B^- production to be observed. They are not and upper limits are presented for the cross sections. Similarly, lack of evidence for A_1^- production is not critical since no A_2^- production is observed. These limits, although smaller than the observed ρ^- cross section, are not yet significantly small to be in conflict with theoretical estimates.

ACKNOWLEDGMENTS

This research was supported primarily by the Energy Research and Development Administration. We would like to thank the staff of the Bevatron and especially J. Brannigan for help during the construction and operation of the experiment and the scanning and measuring staff for their efforts during the analysis of the data.

*Present address: SLAC, Stanford, California.
†Permanent address: University of Michigan, Ann Arbor, Michigan.

[1]See data card listings in Particle Data Group, Rev. Mod. Phys. 48, S1 (1976).
[2]S. Ascoli *et al.*, Phys. Rev. Lett. 26, 929 (1971); Yu. M. Antipov *et al.*, Nucl. Phys. B63, 153 (1973); G. Otter *et al.*, *ibid.* B80, 1 (1974).
[3]R. T. Deck, Phys. Rev. Lett. 13, 169 (1964); E. L. Berger, Phys. Rev. 166, 1525 (1968).
[4]M. J. Emms *et al.*, Phys. Lett. 60B, 109 (1975); F. Wagner *et al.*, *ibid.* 58B, 201 (1975).
[5]E. W. Anderson *et al.*, Phys. Rev. Lett. 22, 1390 (1969).
[6]G. W. Brandenburg *et al.*, Phys. Rev. Lett. 36, 703 (1976); 36, 706 (1976).
[7]W. Tanenbaum *et al.*, Phys. Rev. D 17, 1731 (1978).
[8]The usual distribution of missing mass squared for all events is not shown because the trigger alone does not provide positive identification of the proton. The kinematic fit provides an important contribution to the proton identification.
[9]A. Brabson *et al.*, Phys. Lett. 42B, 283 (1972).

[10]E. W Hoffman *et al.*, Phys. Rev. Lett. 35, 138 (1975).
[11]G. G. G. Massaro *et al.*, Phys. Lett. 66B, 385 (1977).
[12]D. P. Owen *et al.*, Phys. Rev. 181, 1794 (1969).
[13]E. W. Anderson *et al.*, Phys. Rev. Lett. 20, 1529 (1968).
[14]See D. L. Scharre, Ph.D. thesis, LBL Report No. LBL-6149, 1977 (unpublished) for details.
[15]Events with proton trigger acceptance less than 0.15 are eliminated from the data sample. The remaining events are each assigned a weight equal to the inverse of the trigger acceptance.
[16]The background term is parametrized in terms of the expression

$$\left(\frac{d\sigma}{dM}\right)_{\text{background}} = (M - M_{\min})^{\beta_1} (M_{\max} - M)^{\beta_2} \times (\alpha_1 + \alpha_2 M + \alpha_3 M^2 + \cdots),$$

where M is the invariant mass and $M_{\min}$ and $M_{\max}$ are the minimum and maximum kinematically allowed masses. The exponents β_1 and β_2 are small (less than 5) positive numbers. The polynomial coefficients α_1, α_2, $\cdots$ are small in number in order to keep the background simple. It is found that α_i for $i > 3$ can be set equal to zero.
[17]G. Gidal *et al.*, Phys. Lett. B (to be published).
[18]A Monte Carlo simulation is used to estimate the loss of events with trigger acceptance less than 0.15 which are eliminated from the sample.
[19]E. W. Anderson *et al.*, Phys. Rev. Lett. 22, 102 (1969).
[20]The method of moments is used to calculate

$$\rho_{10} = 0.3333 + 2.6422 \langle Y_{20} \rangle,$$
$$\rho_{10} = 2.2882 \langle Y_{21}^* \rangle,$$
$$\rho_{1,-1} = -3.2360 \langle Y_{22}^* \rangle.$$

[21]This correction is less than 20% over the mass region of interest.
[22]An $e^{3u'}$ falloff is assumed for the differential cross section.
[23]The A_1 is assumed to decay totally into $\rho\pi$ and the A_2 is assumed to have a branching fraction of 0.709 into $\rho\pi$.
[24]H. E. Haber and G. L. Kane, Nucl. Phys. B129, 429 (1977).
[25]A. Abashian *et al.*, Phys. Rev. Lett. 34, 691 (1975).
[26]The assumed resonance parameters are $M = 1.228$ GeV and $\Gamma = 0.125$ GeV.